International Journal of Advances in Structural and Geotechnical Engineering

https://asge.journals.ekb.eg/

Print ISSN 2785-9509 *Online ISSN 2812-5142*

Special Issue for ICASGE'19

Assessment of the Efficiency of Rigid Inclusions as a Settlement Control System – Case Study

Amr A. Hemada, Abdullah M. Galaa and Tarek T. Abdel-Fattah

ASGE Vol. 06 (02), pp. 52-67, 2022

Assessment of the Efficiency of Rigid Inclusions as a Settlement Control System – Case Study

Amr A. Hemada[1], Abdullah M. Galaa[2] and Tarek T. Abdel-Fattah[3]

[1] *Associate Professor, Geotechnical Engineering Institute, Housing and Building National Research Center, Egypt.*

E-mail: Hemada2002@yahoo.com

[2]*Associate Professor, Geotechnical Engineering Institute, Housing and Building National Research Center, Egypt.*

E-mail: Abdullah.galaa@hbrc.edu.eg

[2]*Professor, Geotechnical Engineering Institute, Housing and Building National Research Center, Egypt.*

E-mail: Ttabdelfattah@yahoo.com

ABSTRACT

This paper presents a summary of the research work conducted to assess the efficiency of rigid inclusions (RI) as a settlement control system for foundations on soft marine soils (Deltaic formations). The study was conducted at the proposed construction site of a new university located in the coastal city of New Mansoura, North Delta. The RI system comprises unreinforced concrete cast in place displacement piles overlain by a layer of crushed stone-sand mix acting as a load transfer platform (LTP) under the building's footings. To verify the proposed RI system, a specialized contractor conducted full scale trial loading test. The evaluation methodology comprises detailed geotechnical investigation, evaluation of the results of the trial test performed by the specialized contractor, advanced 3D finite element analyses were performed to simulate the trial test (short-term condition) as well as investigation of the long-term behavior of the proposed system (drained condition). The results of analyses have shown that the construction of the rigid inclusion significantly reduced the predicted settlements of the foundation compared to un-piled footing. Reduction in settlements in the undrained and drained conditions are about 30% to 37%, respectively compared to un-piled footing reflecting the efficiency of RI system in controlling foundation settlements. In the undrained condition, the percentage of the load transferred to the rigid inclusions are predicted to be about 63% and 50% for the working and ultimate loading conditions, respectively. While the counterpart percentages in drained condition, are about 76% and 60%.

Keywords: *Rigid inclusions, Full-scale, Loading test, Elasto-plastic analysis, Drained and undrained, Soft soil.*

INTRODUCTION

Settlement control under structures founded on weak soils has always been a serious topic in geotechnical engineering. Two main approaches are usually followed to reduce the expected settlements: (a) improving mechanical properties of the load-bearing soils, and (b) transferring loads to deeper and/or more competent soil layers. Over the past few decades, Rigid Inclusions (RI), also known as Controlled Modulus Columns (CMC), have been receiving increasing attention as an alternative settlement control option.

RI systems relies on the interaction between (1) rigid vertical piles (the inclusions), (2) a load transfer platform (LTP), and (3) the subgrade soil between inclusions. Foundations rest over LTP which acts as a geometric and mechanical discontinuity between the foundation and the inclusions [1]. LTP is an engineered soil layer acting as a mattress usually consisting of granular

soils and horizontal geosynthetic reinforcing elements such as Geogrids. Part of the load is transferred from the foundation to the inclusions through arching effect. In addition to the arching effect, geosynthetic reinforcement creates a membrane effect which transfers loads to the inclusions [2, 3]. Both arching and membrane effects are initiated after the week or soft subgrade soils between the inclusions receives a share of the load and exhibits some settlement. The magnitude of the load transferred to the inclusions through arching and membrane effects depends on the magnitude of settlement of subgrade soil between inclusions. Blanc et al. [3] illustrated the load sharing mechanism in RI systems as shown in Fig. 1. The load sharing mechanisms are not fully comprehended and several studies endeavored to understand such mechanisms. Moreover, studies aimed at understanding the most influencing factors within RI system (RI spacing (S), LTP strength and thickness (H), and characteristics of geosynthetic reinforcement) using experimental and numerical approaches.

It is close to the soil-structure interaction of piled rafts described by [4]. However, bending moments on inclusions are expected to be significantly less than that in the case of connecting to a rigid raft (in piled raft foundations). RI systems also have the advantage of dissipating of horizontal forces by friction between the foundation and LTP.

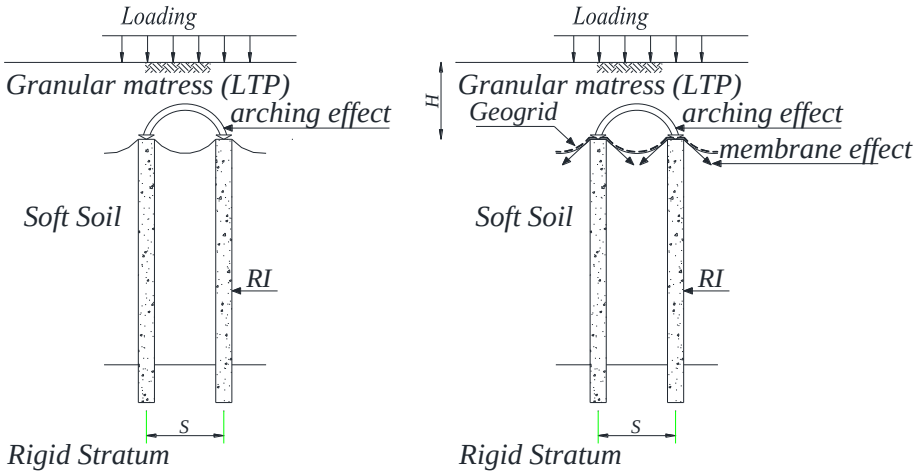

a. Without geogrid **b. With geogrid**

Fig. 1 Load transfer mechanisms in a functioning LTP (after [3]).

The load sharing mechanisms are not fully comprehended and several studies endeavored to understand such mechanisms. Moreover, studies aimed at understanding the most influencing factors within RI system (RI spacing, LTP strength and thickness, and characteristics of geosynthetic reinforcement) using experimental and numerical approaches.

Published experimental approaches included laboratory scale models such as the two-dimensional model developed by [5] and the centrifuge models presented by [3]. There are also true scale experimental models such as those presented by [6 and 2].

Several studies have conducted comparative analyses to assess the performance of numerical tools with analytical methods or physical experimental models. [7 and 5] employed 3D and 2D, respectively, finite difference methods to perform parametric studies to assess the performance of RI systems. 2D and 3D finite element methods were used by [6 and 8] to conduct similar studies. Moreover, [2 and 9] conducted parametric studies using coupled 3D finite and discrete element methods to compare the results with physical laboratory and true scale tests. The analysis model is also similar to the 3D finite element model presented by [10] for simulation of piled raft foundation.

In this paper, a trial test was implemented in New Mansoura City, Egypt, through in-situ loading of a full-scale footing resting on LTP reinforced with a single layer of geogrid on top of cast in place displacement rigid inclusions. This RI system was proposed to support and control settlements of the foundations of a university building resting on loose sand and soft clay deposits. Advanced 3D finite element models were performed to simulate the trial test (short-

term condition) as well as investigation of the long-term behavior of the proposed system which is not covered in the trial test.

PROBLEM STATEMENT

The Egyptian ministry of Housing, Utilities and Urban Communities is currently developing a new urban community called New Mansoura city located north of the Nile Delta, overlooking the Mediterranean coast. In this paper a case study of construction of a proposed university building with high permanent loads is investigated. The area of the project is about 5700 m^2 and the buildings consist of ground floor and four typical floors. The soil at the site of the project comprises a top layer of sand with varying percentages of silt and clay. The thickness of this layer is around 10.0m and it is medium dense to dense. This layer is underlain by a layer of soft to medium silty clay slightly over consolidated (average OCR=1.3). The thickness of this layer is around 6.0m. In case of using conventional raft foundation, the predicted long-term settlement is excessive and is not acceptable as it is expected to have a negative effect on the safety of the building as well as its functionality. Two foundation alternatives were proposed; a) the conventional piled foundation, b) improve or reinforce the soil. As the cost of the conventional piled foundation was high, it was decided to use the second alternative. The soil stratification was ideal for using either piled raft foundation or RI system. Although, piled raft foundation proved to be a successful option in similar soil stratification (as described in [11]), the client entrusted HBRC to assess the efficiency of RI system as it is expected to be more economic. The scope of the assessment included performing additional geotechnical investigation, a full-scale trial test for the RI system and numerical modeling to simulate the trial test in the undrained condition and investigate the drained condition which is not covered by the test.

THE TRIAL TEST

The test on a non-working footing was carried out at the project site up to a test load of 7500kN (double the working load of 3750 kN). The load was incrementally applied at increments of 25% of the working load. Likewise, unloading increments were 25% of the working load. The following sections outline the test loading configuration and the testing procedure.

Test configuration

The test setup and arrangement are explained in writing as follows and portrayed in details in Figures (2) to (7):

- The test level is (+1.6). Eight RI were executed from a working platform level of (+0.6) to a depth of 19.0 m with spacing of 2.0 m and concrete cube strength of 25MPa.
- Rigid inclusions were constructed through driving closed steel pipes using a diesel hammer to a depth of 19.0 m from the working platform level or until refusal (10 blows/10cm), whichever comes first. Concrete is poured into the steel pipes and the pipes were raised as pouring continued.
- A compacted layer of crushed stone was placed up to 0.35 m above the head of the RI.
- A Geogrid layer was placed over the crushed stone layer for reinforcement purpose. Above the geogrid, the load transfer platform (LTP) of 1.0 m thickness consisting of crushed stone-sand mixture was placed and compacted. The LTP was placed on layers 0.25 m thickness, and each layer was compacted and tested. The dry density determined from field testing was larger than 95% of the maximum dry density determined from modified proctor test. A 5m x 5m reinforced concrete footing was constructed over the compacted LTP.
- A hydraulic jack was placed centrally over the footing, then, the reaction system is set up. All reaction platform elements were designed to safely support the required load.
- The settlement was measured using 4 dial gauges mounted on the test footing with their spindles resting on reference beam.

Fig. 2 Steel pipe installation, constructed RI and Geo-grid layer above the RI heads

Fig. 3 Complete trial test setup

¶ Figures 4 and 5 show details of the arrangement of constructed RI system. Soil profile was according to BH1 (nearest borehole).

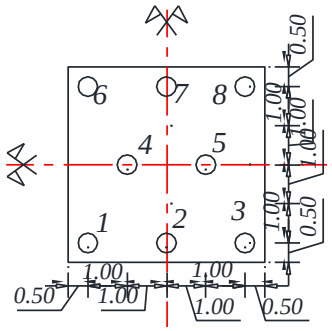

Fig. 4 layout of test footing

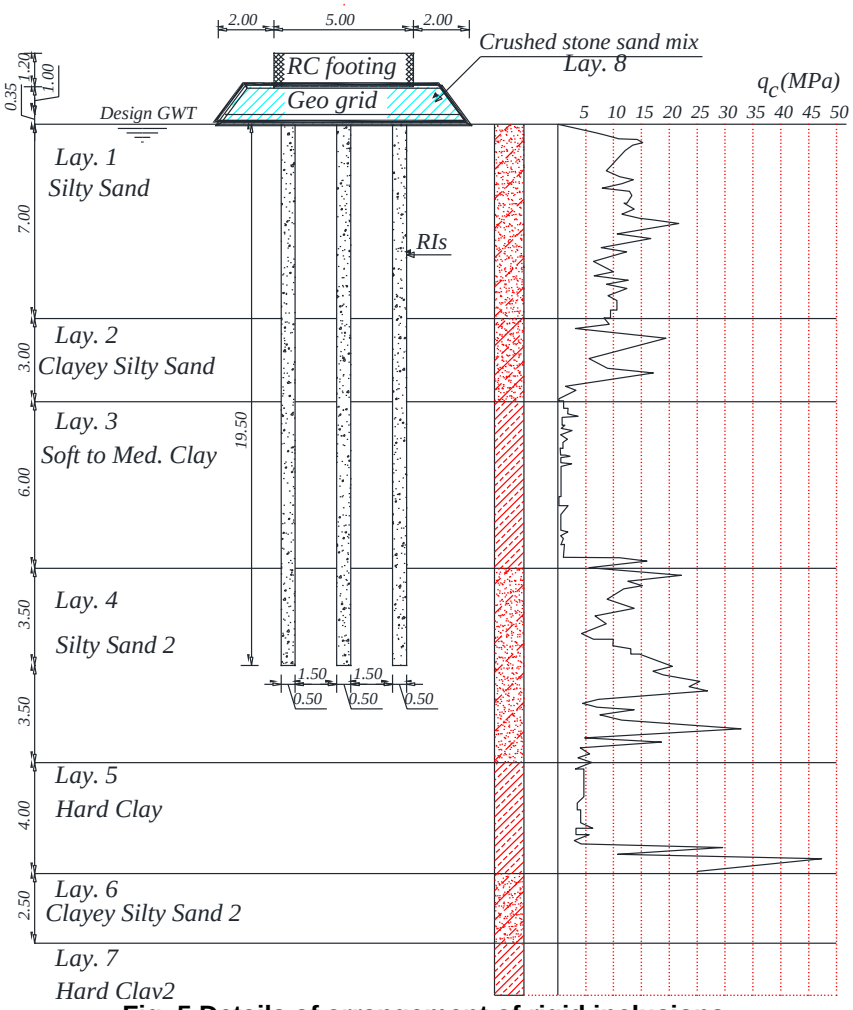

Fig. 5 Details of arrangement of rigid inclusions

Test procedure

The loading/unloading sequence was carried out in accordance with the schedule shown in Table (1). The maximum test load in this case is twice the required working load (3750 kN). Loading and measurements were performed under supervision of HBRC.

Table 1: Loading procedure table

Stage	Time (min)	Load (%)	Load (kN)	Stage	Time (min)	Load (%)	Load (kN)
1	0	0	0	14	3×60	125	4687.5
2	1×60	25	937.5	15	3×60	150	5625
3	1×60	50	1875	16	3×60	175	6562.5
4	1×60	75	2812.5	17	24×60	200	7500
5	24×60	100	3750	18	15	175	6562.5
6	30	75	2812.5	19	15	150	5625
7	30	50	1875	20	15	125	4687.5
8	30	25	937.5	21	15	100	3750
9	30	0	0	22	15	75	2812.5
10	30	25	937.5	23	15	50	1875
11	30	50	1875	24	15	25	937.5
12	30	75	2812.5	25	4×60	0	0
13	30	100	3750				

Test results

The load settlement curve and summary table obtained from the results of the trial load test are shown in Figure 6. The proposed design working and ultimate loads for the trial footing was 3750 kN and 7500 kN, respectively.

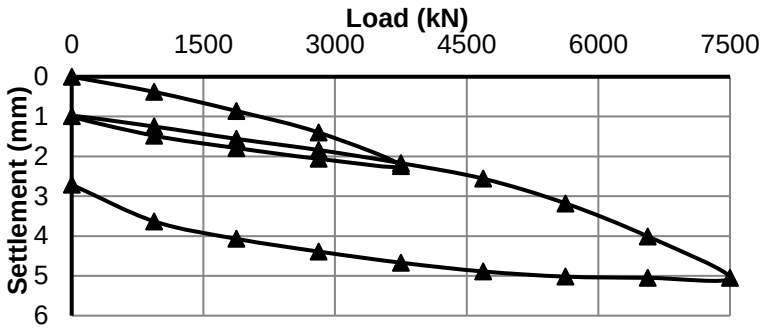

Fig. 6 Measured Load ï Settlement relationship

GEOTECHNICAL INVESTIGATION

Additional geotechnical investigation program took place including five CPTU tests of a 30.0 m depth and four boreholes of 30.0 m depth. Field vane shear tests were performed in clay layers every 3.0 m. Distribution of CPTU test points and boreholes are presented in Figure 7.

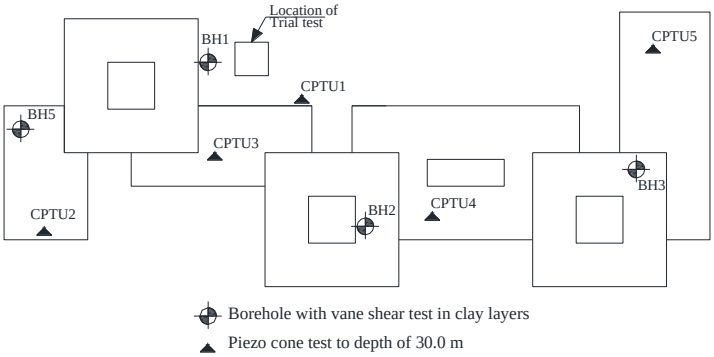

Fig. 7 Location of proposed CPTU test points and boreholes.

SUBSURFACE CONDITIONS

According to the results of the geotechnical investigation carried out at the site of the project, the stratification may be summarized as shown in Figure 5.

Soil Material parameters

The soil material parameters used in the FE models are represented in the following sections.

a. Shear-strength parameters:

The effective friction angle of the soil, f from the values of the cone resistance (q_c) using relationship given by [12] and [13] as follows:

$$\emptyset' = 17.6° + 11 \times \log(q_{t1})$$

Where, q_{t1} is a stress-normalized cone resistance given by:

$$q_{t1} = \frac{q_c/\sigma_{atm}}{\sqrt{\frac{\sigma'_{vo}}{\sigma_{atm}}}}$$

Where, atm = atmospheric pressure = 101.325 kPa, and s'vo = effective overburden stress.

and a very small value of 1 kPa is used in numerical models.

b. Deformation parameters

The secant value of the pseudo-elastic deformation modulus, E_{50}, is calculated from values of the cone resistance (q_c) using the following relationship [13]:

$$E_{50} = \alpha \times q_c$$

with the common values for a in the range of 2 < a < 10. The values of a are taken as: a=5 for sandy soils and a=3 for silt and clay. For Modified Mohr-Coloumb soil model (MMC) used in the FE analyses, the reference value of E_{50} , known as E_{50}^{ref} is calculated as follows:

$$E_{50}^{ref} = E_{50} \times \left(\frac{\sigma'_h}{p_{ref}}\right)^m$$

The reference values for the unloading-reloading modulus, E_{ur}^{ref}, and the one-dimensional modulus, E_{oed}^{ref}, are taken as the defaults given by DIANA program as follows:

$$E_{ur}^{ref} = 3 \times E_{50}^{ref}$$

$$E_{oed}^{ref} = E_{50}^{ref}$$

In all analyses, the value of the reference pressure is taken as, p^{ref} =100 kPa

The following table represent values of predicted soil parameters used in the analysis:

Table 2: Soil parameters for the FE analysis.

Parameter	Soil Layer							
	Lay.1	Lay.2	Lay.3	Lay.4	Lay.5	Lay.6	Lay.7	Lay.8*
Bulk unit weight (kN/m^3)	18	18	16	19	18	19	18	18.5
Cohesion C (kPa)	5	1	2	1	2	1	2	15
Friction angle, f °	37	34	25	38	30	37	32	40
E_{50}^{ref} or E_{50} (MPa)	50	50	1.3	60	15	60	17.5	150
E_{oed}^{ref} (MPa)	--	--	1.05	--	--	--	--	--
E_{ur}^{ref} (MPa)	--	--	4	--	--	--	--	--
Poissonôs r	0.3	0.3	0.2	0.3	0.3	0.3	0.3	0.3
p^{ref} (kPa)	--	--	100	--	--	--	--	--
R_f, (-)	--	--	0.9	--	--	--	--	--
Preconsolidation. pressure (kPa)	--	--	102.6	--	--	--	--	--
At rest coefficient, K_o	0.5	0.5	0.65	0.4	0.5	0.4	0.47	0.5

* A 1.0 m thick (LTP) layer composed of crushed stone: sand mix at a ratio 2:1.

DETAILED 3D NONLINEAR FE MODEL:

In the model(s) performed to simulate the loading test, the existing soil-structure was appropriately modeled making use of the performed field and laboratory geotechnical investigation. To determine the effect of construction history, different construction phases were simulated via the phased-analysis option. Soil strata were modeled using Mohr Coulomb (MC) elasto-plastic model for granular soils including the load transfer platform and hard clays, while Modified Mohr Coulomb (MMC) elasto-plastic model is used for soft to medium cohesive soils. Both rigid inclusions and reinforced concrete rigid footing are modeled as linear elastic. Friction type interface elements are used to model the interface between shafts of RI and surrounding soil. The yield condition of the MC and MMC are shown in Figures 8 and 9, respectively. The FE analyses were carried out using the general purpose FE program DIANA® VER. 10.3 (TNO DIANA BV. 2019).

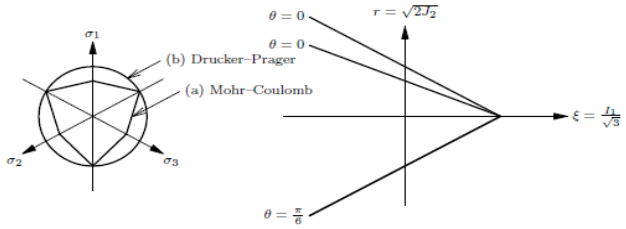

Fig. 8 Mohr-Coulomb Yield Condition

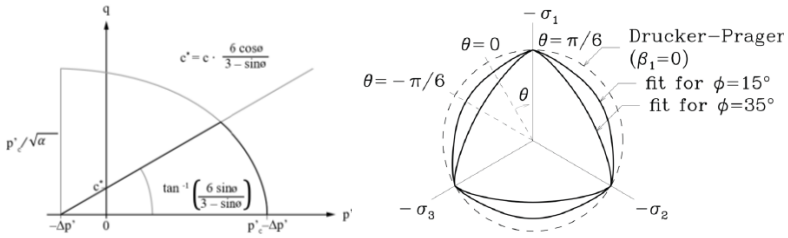

Fig. 9 Modified Mohr-Coulomb Yield Condition

Material Properties and Design Parameters

The material properties and design parameters for RI and reinforced concrete footing used in the analyses are listed in Table (3). Both are modeled as Linear elastic.

Table 3 Concrete material properties

Parameter	Rigid inclusions	Rigid footing
Total unit weight (kN/m^3)	24	24
	2.0E+7	2.0E+7
n	-	0.20
Interface reduction factor, (R)	1	-

Description of the 3D Finite Element Model

The full 3D finite-element mesh of the problem is shown in Figure 10 showing geometry points, loads and boundary conditions. Only one quarter of the problem is modeled using FE due symmetry in x and y directions. Seven soil layers, in addition to the load transfer platform were modeled using solid elements. Phased analyses were conducted to simulate the construction sequence in both short-term (undrained) and long-term (drained) conditions. The FE model consisted of 29201 nodes and 8172 solid elements.

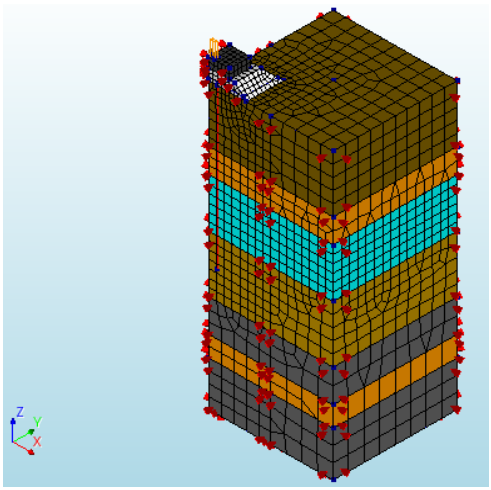

Fig. 10 The 3D FE mesh showing geometry points, loads and boundary conditions

Results of analyses

a. Undrained condition

Figures 11 and 12 show the contours of vertical displacement at design working and ultimate loads, respectively. Maximum predicted settlement at center of footing was 7.55 mm and 16.52 mm at working and ultimate loads, respectively. Figures 13 presents the predicted load-settlement relationship for points at center and corner of the footing. It can be seen from Figure 13 that the maximum differential settlement is about 0.75 mm and 1.12 mm (corresponding to a tilt of about 2.12×10^{-4} and 3.17×10^{-4}) at design working and ultimate loads, respectively. The predicted undrained settlement at corner of footing was 6.95 mm and 15.4 mm at working and ultimate loads, respectively. The measured values in the loading test at the corners of the footing were 2.24 mm and 5.05 mm at working and ultimate loads, respectively. Predicted values are considerably higher than measured values due to probable settlement of reference beams and measurement fluctuation caused by temperature changes on restrained reference beams from both sides. The FE model shows linear settlement at the location of supports of the reference beams. Therefore, the measured values were corrected to account for reference beams settlement. The corrected settlement at corner of footing was 4.74 mm and 10.05 mm at working and ultimate loads, respectively. Figure 14 presents a comparison of the measured, corrected and predicted settlement in the undrained condition. The difference between the corrected and predicted response could be attributed to effects of temperature fluctuations on the restrained beams and to the kentledge loading system.

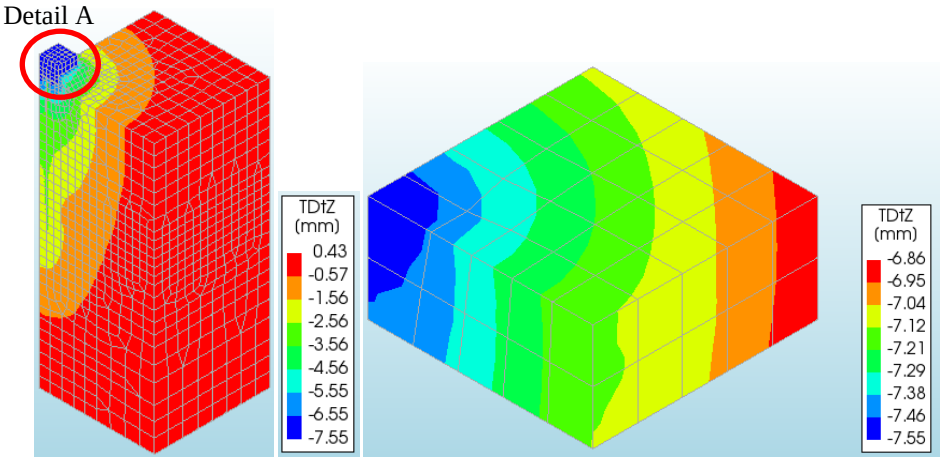

b. Full model **b. Detail A**

Fig. 11 Contours of vertical displacement at design working load ï undrained condition

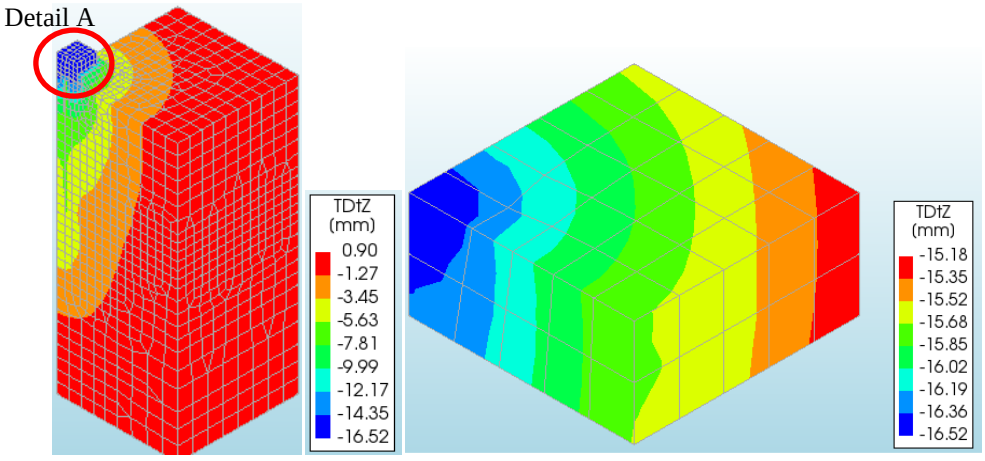

c. Full model **b. Detail A**

Fig. 12 Contours of vertical displacement at design ultimate load ï undrained condition

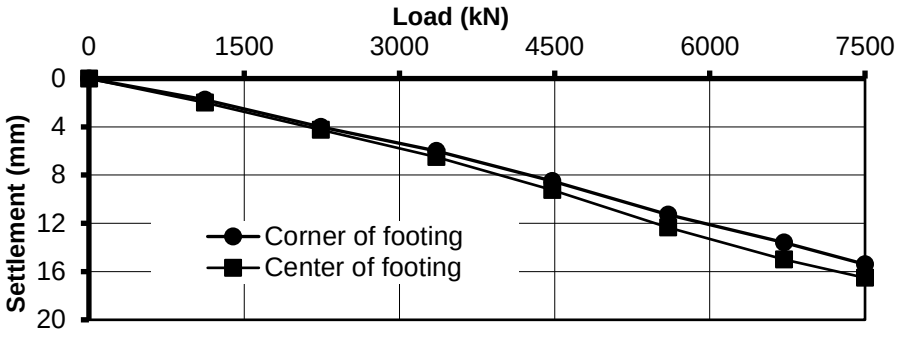

Fig. 13 Load-settlement relationship ï undrained condition

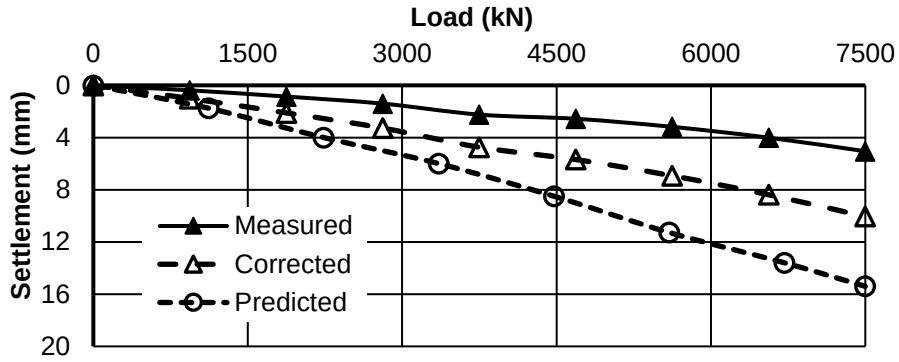

Fig. 14 Comparison of measured and predicted settlement at footing corner - undrained

Figure 15 shows the distribution of axial forces along shaft of the corner RI at both working and ultimate loads, respectively. Maximum predicted loads are 316.7 kN and 494.25 kN at both working and ultimate load, respectively. Figure 16 shows the distribution of axial forces along the shaft of the edge and interior RIs at both working and ultimate loads, respectively. Maximum predicted loads are 278.48 kN and 462.76 kN at both working and ultimate load, respectively. Due to symmetry, only half of each of edge and interior piles is modeled and consequently the output straining actions obtained shall be multiplied by two. It can be seen from the distribution of axial force along the pile shaft and from Figure 17 that the maximum load is located below the pile head. This distribution describes the characteristic load sharing mechanism between soil and RIs resulting from soil arching effect caused by the relative stiffness between RI and supporting soil. It is worth
negligible.

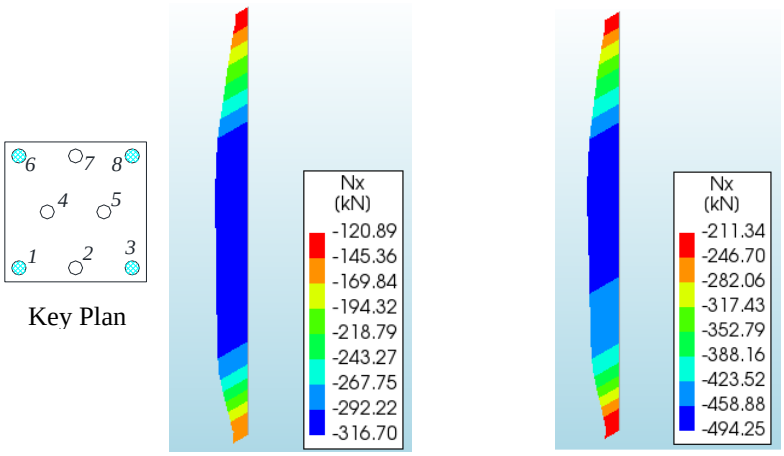

a. At deign working load b. At design ultimate load

Fig. 15 Distribution of axial load along corner RI ï undrained condition

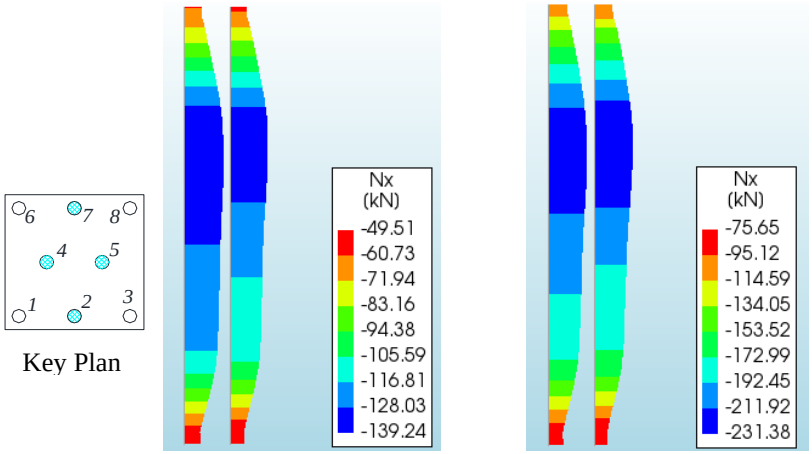

b. At deign working load **b. At design ultimate load**

Fig. 16 Distribution of axial load along edge and interior RIs ï Undrained condition

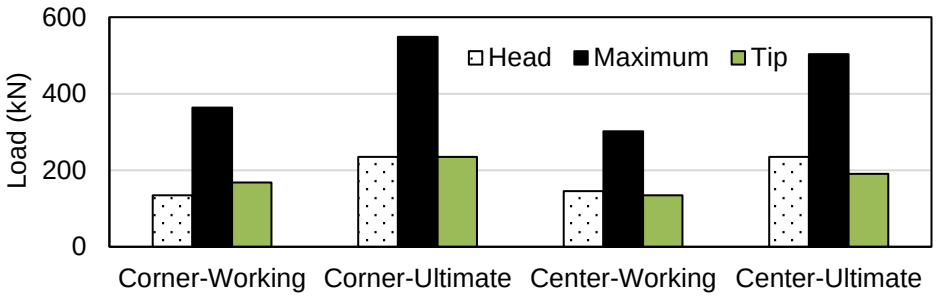

Fig. 17 Maximum axial load compared to axial load at head and tip - undrained condition

d. Drained condition

Figures 18 and 19 show the contours of vertical displacement at working and ultimate loads, respectively. Maximum predicted settlement at center of footing was 11.06 mm and 23.65 mm at working and ultimate loads, respectively. Figure 20 presents the predicted load-settlement relationship for points at center and corner of the footing. It can be seen from Figure 20 that the maximum differential settlement is about 0.75 mm and 1.15 mm (corresponding to a tilt of about 2.12×10^{-4} and 3.25×10^{-4}) at design working and ultimate loads, respectively.

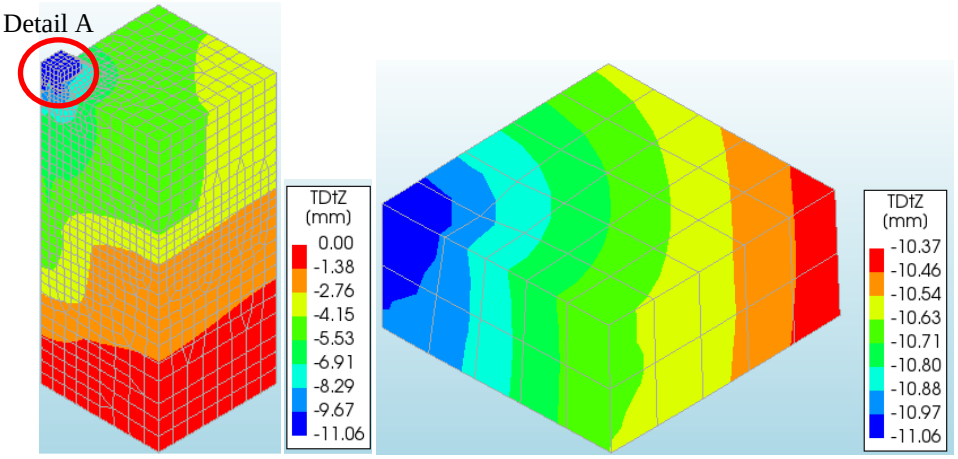

a. Full model **b. Detail A**

Fig. 18 Contours of vertical displacement at working load level–drained condition

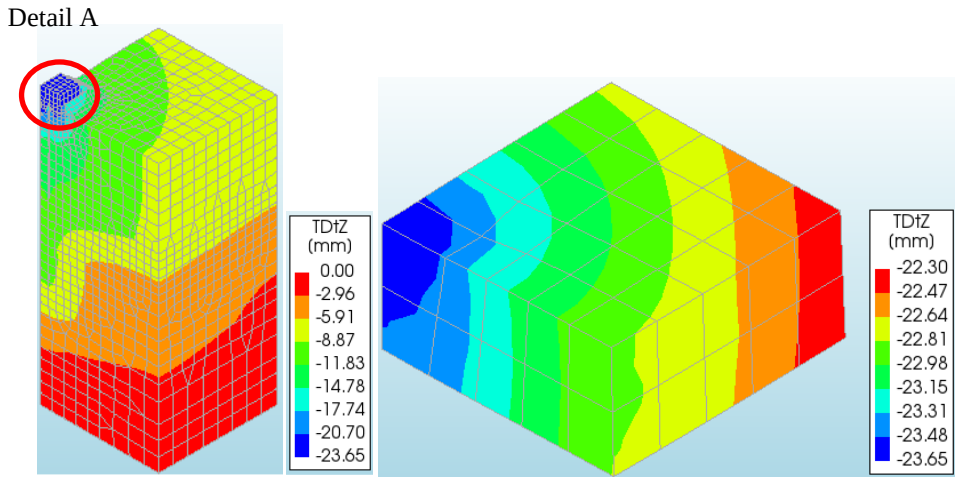

a. Full model **b. Detail A**

Fig. 19 Contours of vertical displacement at ultimate load level–drained condition

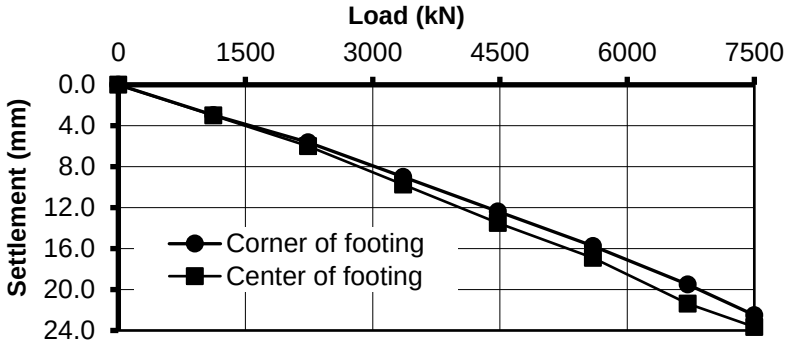

Fig. 20 Load-settlement relationship ï drained condition

Figure 21 shows the distribution of axial forces along shaft of corner RI at both working and ultimate loads, respectively. Maximum predicted loads are 397 kN and 615.05 kN at both working and ultimate loads, respectively. Figure 22 shows the distribution of axial forces along the shaft of the edge and interior RIs at both working and ultimate loads, respectively. Maximum predicted loads are 316.16 kN and 518.72 kN at both working and ultimate loads, respectively. The same characteristic load sharing mechanism observed in undrained condition, is noticed. It negligible. Figure 23 presents a comparison between maximum axial load and axial load at head and tip.

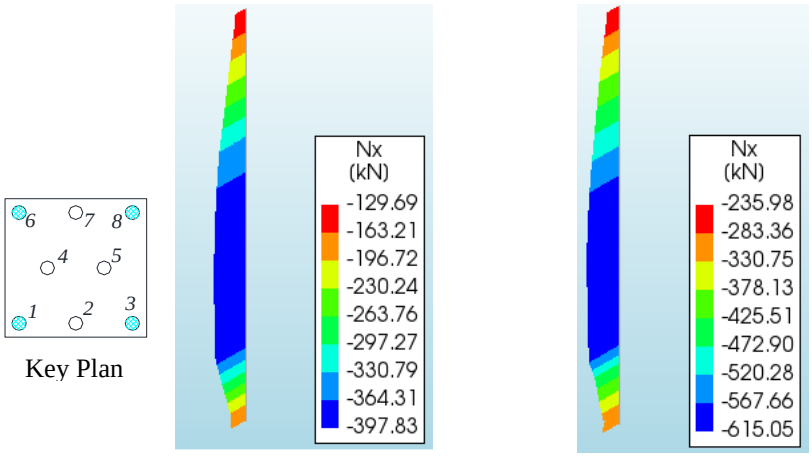

a. At deign working load **b. At design ultimate load**

Fig. 21 Distribution of axial load along corner RI ï drained condition

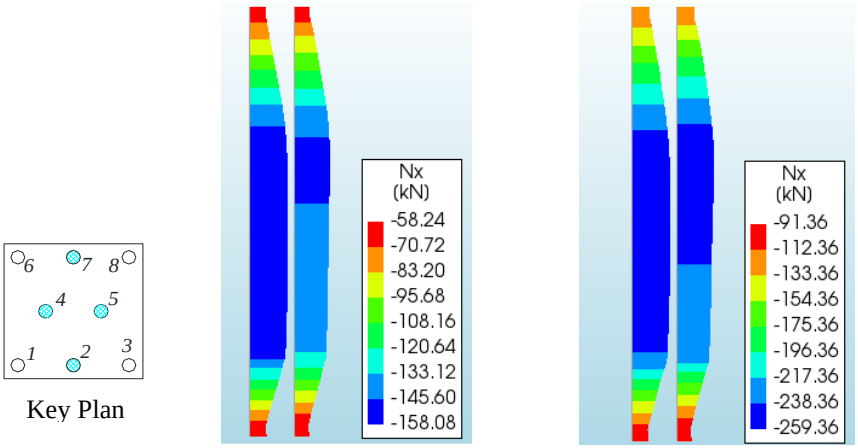

a. At deign working load **b. At design ultimate load**

Fig. 22 Distribution of axial load along edge and interior RIs ï drained condition

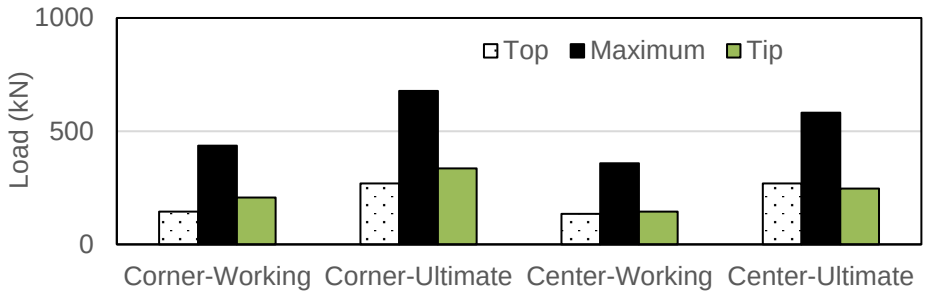

Fig. 23 Maximum axial load compared to axial load at head and tip - drained condition

Un-piled footing

For comparison purpose, un-piled footing (without rigid inclusions) was modeled in both drained and undrained conditions.

a. Undrained condition

Figure 24 shows the contours of vertical displacement at working and ultimate loads, respectively. Maximum settlement at center of footing was 11.07 mm and 26.29 mm at design working and ultimate loads, respectively. Figure 25 presents load-settlement relationships for points at center and corner of the footing. It can be seen from the load-settlement relationships that failure signs started to appear in case of un-piled footing, while considerable reduction in settlement can be observed in RI system.

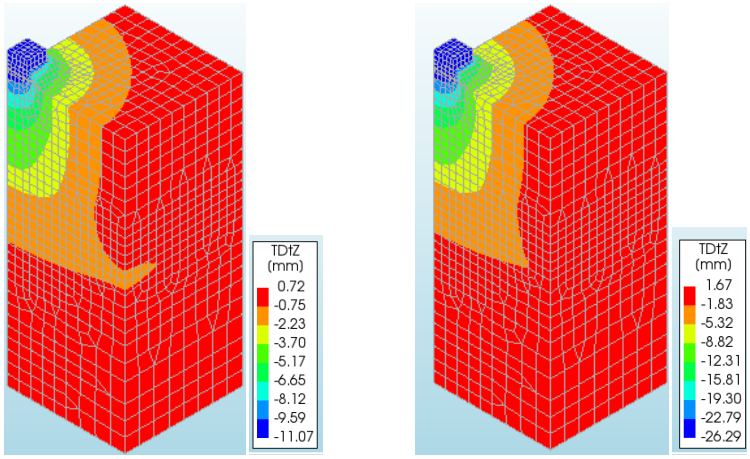

a. At deign working load **b. At design ultimate load**

Fig. 24 Contours of vertical displacement ï undrained condition

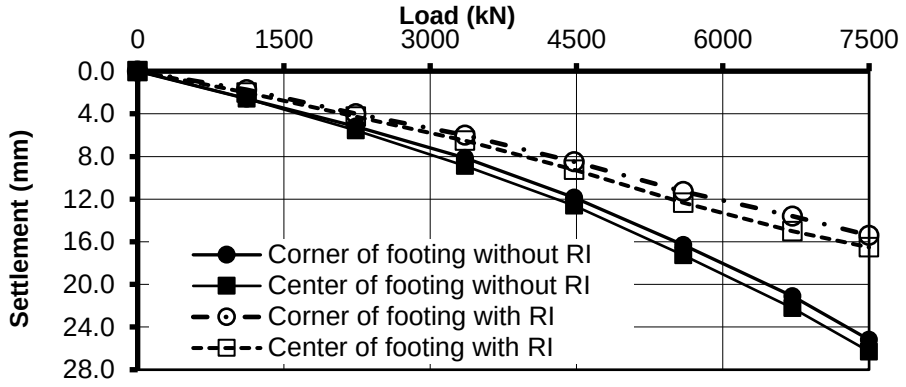

Fig. 25 Load-settlement relationship ï undrained condition

b. Drained condition

Figure 26 shows the contours of vertical displacement at working and ultimate loads, respectively. Maximum settlement at center of footing was 15.86 mm and 36.95 mm at design working and ultimate loads, respectively. Figure 27 presents load-settlement relationships for points at center and corner of the un-piled footing compared to RI system. It can be seen from the load-settlement relationships that failure signs started to appear in case of un-piled footing, while considerable reduction in settlement can be observed in RI system.

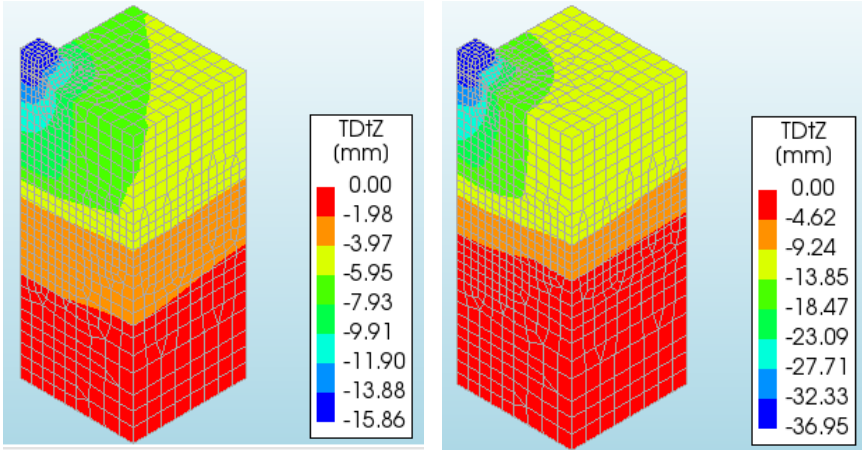

a. At deign working load **b. At design ultimate load**

Fig. 26 Contours of vertical displacement ï drained condition

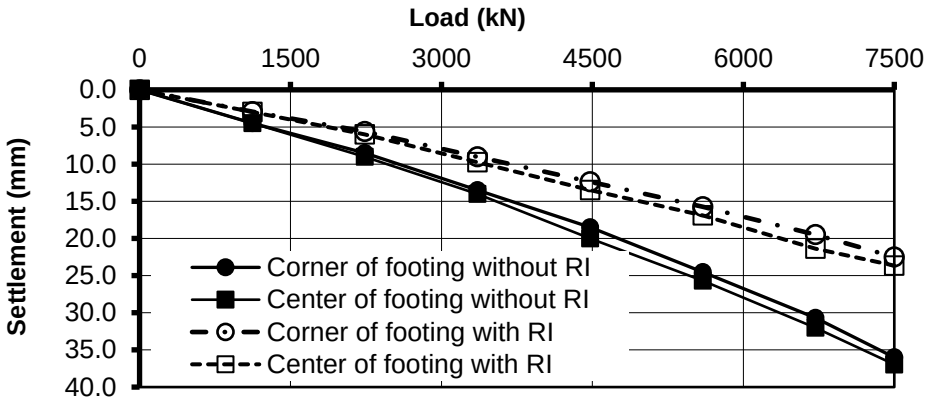

Fig. 27 Load-settlement relationship ï drained condition

SUMMARY AND CONCLUSION

In this paper, a methodology for the assessment of the performance of rigid inclusions as settlement control system has been presented. A trial test on a full-scale RI system was conducted in an area with soft marine deposits coupled with detailed numerical analyses in both drained and undrained conditions. The following can be concluded from the results of the assessment:

- Construction of the RI system reduced the predicted settlements of the foundation at design working load by about 32% and 30% in undrained and drained conditions, respectively, and at design ultimate load by about 37% and 36% in undrained and drained conditions, respectively, compared to un-piled footing.
- Load is transferred from soil to RIs by arching mechanism.
- The maximum values of load transferred to the rigid inclusions for both design working and ultimate loading conditions are considerably lower than the structural capacities of the rigid inclusion. In the undrained condition, the percentage of the test loads transferred to the rigid inclusions are estimated to be about 63% and 50% for the working and ultimate loading conditions, respectively. While in drained condition, the percentage of the test loads transferred to the rigid inclusions are estimated to be about 76% and 60% for the working and ultimate loading conditions, respectively.
- The rigid inclusions system in both undrained and drained conditions shows smooth behavior between the level of loading and the resulting settlement. Neither excessive settlement nor reduced stiffness were predicted for both conditions.
- The predicted capacity of the system could be increased or number of rigid inclusions reduced and consequently reduce cost of foundation.
- It is recommended for future trial loading tests to consider that the Kentledge loading may have an impact on the measured response especially for relatively big size footings. It is recommended to use tension piles or anchors for the reaction system.

Units:

The International system of units (SI) should be used; Equivalents in other units may be given in parentheses

REFERENCES

1. inclusion ground improvement: ASIRI National Project. Presses des Ponts, Paris.
2. reinforced by piles and geosynthetics Numerical and experimental studies dealing with the transfer of load on -2), pp. 78-91.
3. Blanc, M., Rault, G., Thorel, L., & Almeida, M. (2013),

   Geotextiles and Geomembranes, Vol. 36, pp. 92-105.
4. Katzenbach, R., Moorman, C. and Reul, O. (1999), "Ein beitrag zur klarung des tragverhaltens von kombinierten pfahl-plattengrundungen". In Rodatz, W. (ed.), Pfshl-symposium, Mitteilung des institutes fur grundbau und Boden-mechanik, TU Braunschweig, Vol. 60, pp. 263-299.
5. Jenck, O., Dias, D., & Kastner, R. (2005), Soft ground improvement by vertical rigid piles two-dimensional physical modelling and comparison with current design methods Soils and Foundations, Vol. 45(6), pp. 15-30.
6. Nuñez, M., Dias, D., Kastner, R., & Poilpré, C. (2008), Soft ground improved by rigid vertical piles Experimental and numerical study of two real cases in France Proceedings of the 6th International Conference on Case Histories in Geotechnical Engineering, Arlington, VA, August 11-16, 2008.

7. Naughton, P. J., & Kempton, G. T. (2005) Comparison of analytical and numerical analysis design methods for piled embankments In Contemporary Issues in Foundation Engineering, pp. 1-10.
8. ngs of the 9th European Conference on Numerical Methods in Geotechnical Engineering, Porto, Portugal, 25-27 June 2018
9. Chevalier, B., Villard, P., & Combe, G. (2011), Investigation of load-transfer mechanisms in geotechnical earth structures with thin fill platforms reinforced by rigid inclusions International Journal of Geomechanics, Vol. 11(3), pp. 239-250.
10. Hemada, A.A and Akl, A.Y. (2007), "Contribution to three-dimensional finite-element modelling of piled raft foundation system", Journal of Soil Mechanics and Foundation Engineering, The Egyptian Geotechnical Society, Volume 18 (1).
11. Abdel-Fattah, T. T. and Hemada, A. A. (2014), Use of creep piles to control settlement of raft foundation on soft clay case study In Proceedings of 8th Alexandria international conference on structural and geotechnical engineering, Alexandria, pp. 89-109.
12. Kulhawy, F.H. and Mayne, P.W. (1990), Estimating Soil Properties for Foundation Design EPRI Report EL-6800, Electric Power Research Institute, Palo Alto: pp. 306.
13. Interpretation of geotechnical parameters from seismic piezocone tests In Proceedings of the 3rd International Symposium on Cone Penetration Testing (CPT'14, Las Vegas), ISSMGE Technical Committee TC 102, Edited by P.K. Robertson and K.I. Cabal: p 47-73.